MMTO Technical Memorandum #03-5
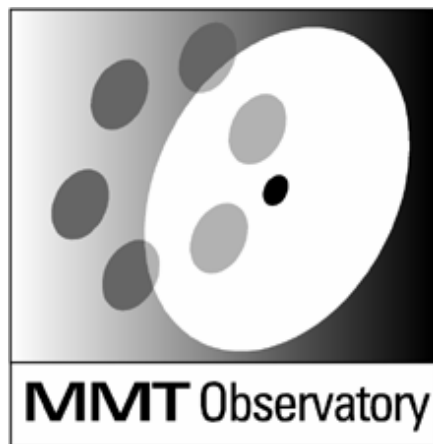
Segmented Zero-Deviation Cross-Dispersion Prisms
for the Hectochelle Multiobject Spectrograph

D. G. Fabricant, A. Szentgyorgyi, H. W. Epps

Segmented Zero-Deviation Cross-Dispersion Prisms for the Hectochelle Multiobject Spectrograph

DANIEL G. FABRICANT AND ANDREW SZENTGYORGYI

Center for Astrophysics, 60 Garden Street, Cambridge, MA 02138; dfabricant@cfa.harvard.edu, saint@cfa.harvard.edu

AND

HARLAND W. EPPS

UCO/Lick Observatory, University of California, Santa Cruz, CA 95064; epps@ucolick.org

ABSTRACT. We present a design for a zero-deviation cross-disperser to be used with Hectochelle, a fiber-fed echelle spectrograph. Hectochelle was originally designed to be operated as a multiobject spectrograph in a single order (or overlapping orders) selected with order-separating filters. With cross-dispersion, the multiplex advantage can be traded for spectral coverage using order-separating filters and masks at the fiber slit. The options range from using two fibers delivering the full 365–980 nm passband to 240 fibers delivering a single order (~10–20 nm). The cross-disperser is a novel segmented prism design, which is compact, efficient, and economical compared to a monolithic zero-deviation prism. Conveniently, the cross-disperser can be mounted in the existing Hectochelle spectrograph without mechanical modifications or optical realignment.

1. INTRODUCTION

Multiobject spectrographs speed the acquisition of astronomical spectra by factors of up to several hundred compared with single-slit instruments by using the full format of two-dimensional detectors. Unfortunately, multiobject spectrographs that use echelle gratings to achieve high dispersion are typically restricted to a small free spectral range (perhaps 10–20 nm) selected with order-separating filters because the available detector area is devoted to multiple spectra. Many scientific programs, especially high-stability radial velocity studies, would benefit from a flexible trade-off between multiplex advantage and spectral coverage. Here, we describe a compact style of cross-disperser that is compatible with fiber-fed multiobject echelle spectrographs and that allows such a trade-off.

We are just about to commission a fiber-fed multiobject echelle spectrograph at the converted MMT: Hectochelle (Szentgyorgyi et al. 1998). This instrument was designed to obtain spectra from 240 optical fibers, each in a single diffractive order selected with order-separating filters. Recently, we began to consider how we might add cross-dispersion to Hectochelle to increase its versatility.

Cross-dispersion can be provided by either gratings or prisms, but prism cross-dispersion usually offers greater throughput and more uniform order separation (Vogt 1987; Walker, Diego, & Bingham 1990). The major concern with prism cross-dispersion is that large prisms are required to provide adequate order separation. When large amounts of cross-dispersion are required to accommodate a long slit, prism cross-

dispersion can become impractical (Vogt et al. 1994). With fiber-fed instruments, the required order separation is relatively modest and is compatible with prism cross-dispersion.

2. ZERO-DEVIATION CROSS-DISPERSION WITH SEGMENTED PRISMS

We arrived at a cross-disperser design that uses segmented, zero-deviation prisms and requires no modification to the existing spectrograph mechanical layout. A zero-deviation prism leaves a chosen central wavelength undeviated while dispersing the spectrum sufficiently to separate the diffractive orders at the focal plane. Zero-deviation prisms are produced by coupling prisms of high- and low-dispersion glasses; the apex angles of the two coupled prisms are chosen to provide the desired zero-deviation condition, and elsewhere light is dispersed according to the dispersion difference between the two glasses. Zero-deviation prisms are not typically used for cross-dispersion because they offer considerably less total dispersion than conventional prisms of the same size. In our case, where the zero-deviation condition is a mechanical requirement, we find that a monolithic zero-deviation prism would be too large to fit in the available space. Furthermore, a thick, monolithic zero-deviation prism made from appropriate glasses would absorb blue light significantly.

We realized that a zero-deviation prism becomes practical if it is formed in stacked segments as shown in Figure 1. The number of prism pairs in the stack is a compromise: as the number of prism pairs is increased, the mass, size, and internal
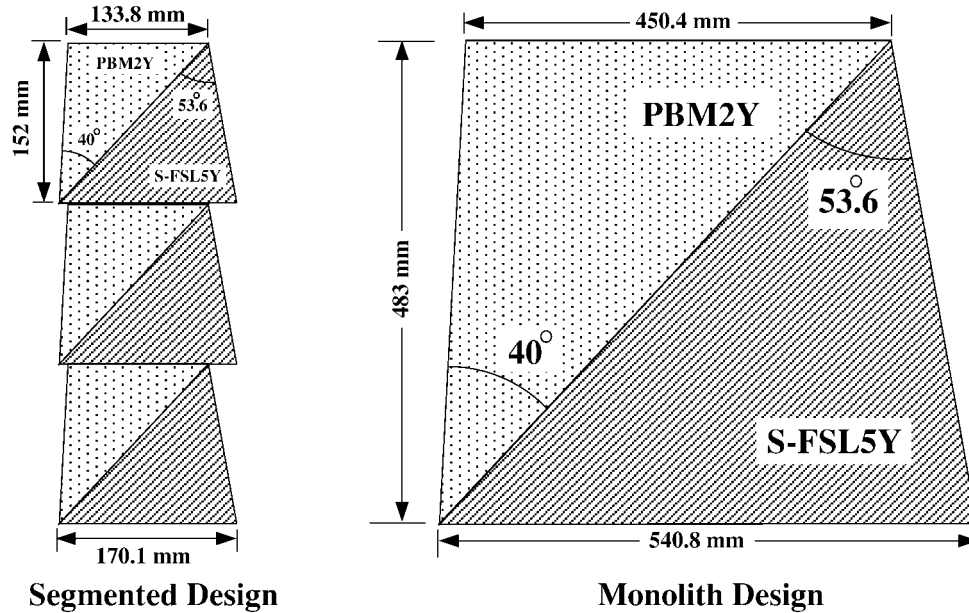
FIG. 1.—Segmented zero-deviation prisms are much less bulky than monolithic prisms. Here we compare the dimensions of a monolithic cross-disperser large enough for the Hectochelle and the equivalent segmented prism stack.

absorption in the glass all decrease, but the number of gaps between the prism pairs increases. At the position of the Hectochelle cross-disperser a monochromatic beam has an area of 8.6×10^4 mm^2, while a 2 mm bevel will occult 2×10^3 mm^2, causing ~2% vignetting in the stack of three prism pairs shown in Figure 1.

Walker et al. (1990) have described using segmented prisms to replace conventional cross-dispersion prisms, and they present several possible segment geometries. Our zero-deviation design avoids large dead areas and gaps in the pupil without the mechanical complexities described by Walker et al. (1990), but produces considerably less order separation than their designs. Figure 2 shows the optical path through the stacked zero-

deviation segments. With an appropriate geometry, the beams proceed through the prism pair with little vignetting from the prism tops or bottoms. To suppress ghost image formation, it is desirable to arrange the prism so that no interface is normal to the beam direction.

3. ZERO-DEVIATION PRISM DESIGN

3.1. Mechanical Constraints

The layout of the Hectochelle spectrograph is shown in Figure 3; the spectrograph is mounted on a 1.7 m × 5.5 m optical bench. The cross-disperser must be placed somewhere in the parallel beam, i.e., between the collimator and the first optical
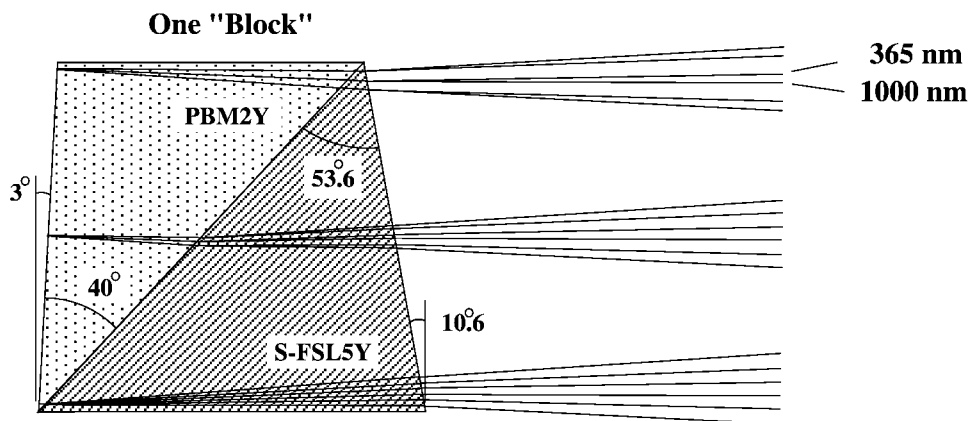

FIG. 2.—Properly designed segmented zero-deviation prisms are almost free from vignetting. Rays for the extreme field angles and extreme wavelengths in the passband are indicated.
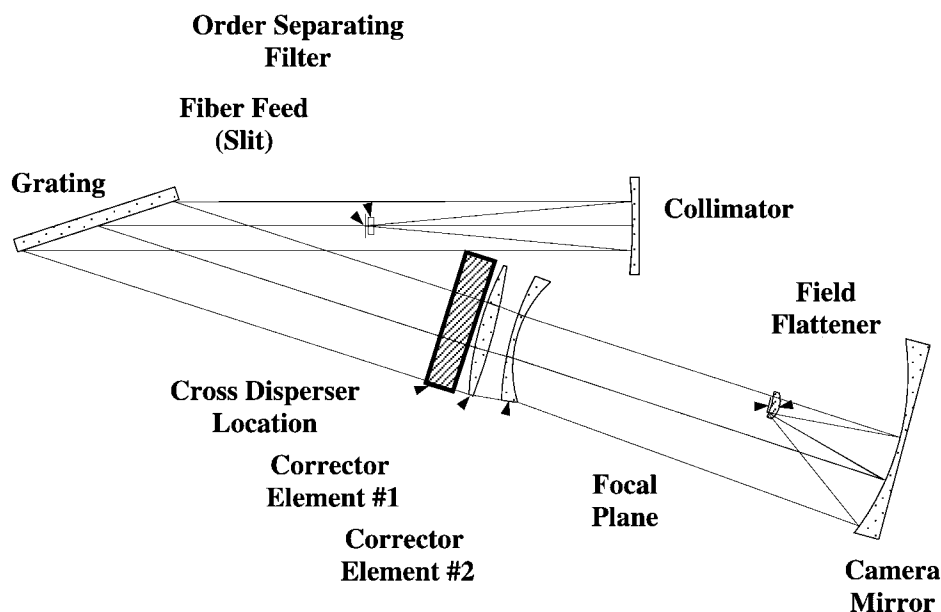
FIG. 3.—Layout of the Hectochelle strongly constrains the cross-disperser design if the cross-disperser is to be fitted in without modifications to the spectrograph and without vignetting the beam in the collimator arm of the spectrograph.

element of the camera. Inspection of the layout indicates that the only possible cross-disperser location is just before the camera corrector doublet. To avoid vignetting the beam in the collimator arm of the spectrograph, the thickness of the prisms must be no more than 175 mm. Here the compact format of the segmented cross-disperser is essential: a monolithic cross-disperser would not fit. At the selected position for the cross-disperser, the overall beam footprint fits within a rectangle 0.61 m wide and 0.48 m tall. Each monochromatic beam from a single fiber is a 0.43 m × 0.25 m ellipse (see Fig. 4).

3.2. Choice of Prism Glasses

To form the zero-deviation prisms, we combine a glass of low dispersion (high Abbe number) with one of high dispersion (low Abbe number). The chosen glasses should transmit well across the passband of the spectrograph and provide adequate cross-dispersion at the red end of the passband. It is desirable to match the coefficients of thermal expansion of the glasses to avoid thermally induced stress in bonded prism pairs.

The Ohara i-line glasses offer excellent transmission in the UV and are widely used in astronomical instrumentation. PBM2Y has the lowest Abbe number, ν_d, of the i-line glasses, and S-FPL51Y the highest, so these are a logical starting point:

$$\nu_d \equiv \frac{n_d - 1}{n_F - n_C},$$

where n_F, n_d, and n_C are the refractive indices at 486.1, 587.6, and 656.3 nm, respectively. Unfortunately, S-FPL51Y has an

anomalously high thermal expansion, nearly 60% higher than the typical i-line glass. S-FSL5Y has the second-highest Abbe number of the i-line glasses and matches the thermal expansion of PBM2Y to within 4%.

We can examine the dispersion curves in more detail, since we know that order separation at the red end of the spectrum is the crucial issue. In the small angle approximation to Snell's law, the deviation δ of the prism pair is

$$\delta = -[n_1(\lambda) - 1]\theta_1 + [n_2(\lambda) - 1]\theta_2,$$

where n_1 and n_2 are the refractive indices of the two components and θ_1 and θ_2 are their angles. The zero-deviation condition at λ_0 in the small angle approximation is

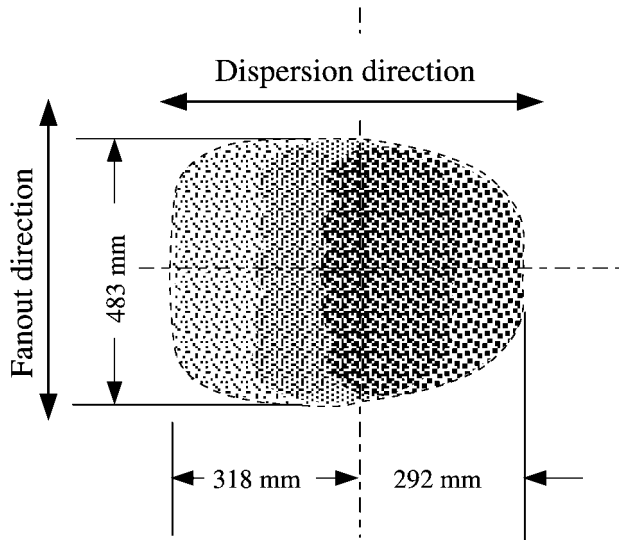$$\frac{\theta_1}{\theta_2} = \frac{n_2(\lambda_0) - 1}{n_1(\lambda_0) - 1}.$$

Combining these, we get

$$\delta \propto -\frac{n_1(\lambda) - 1}{n_1(\lambda_0) - 1} + \frac{n_2(\lambda) - 1}{n_2(\lambda_0) - 1}.$$
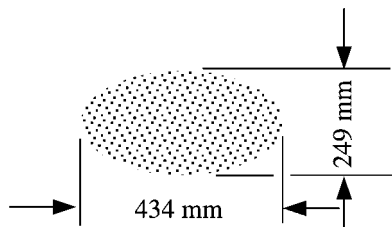
The difference in angle Δ at two wavelengths closely spaced wavelengths in the red, λ_t and λ_s, is

$$\Delta \propto -\frac{n_1(\lambda_s) - n_1(\lambda_t)}{n_1(\lambda_0) - 1} + \frac{n_2(\lambda_s) - n_2(\lambda_t)}{n_2(\lambda_0) - 1}. \qquad (1)$$

The two terms on the right are reciprocal Abbe numbers defined

Dispersion direction

Fanout direction

483 mm

318 mm   292 mm

Beam Pattern at Cross Disperser

249 mm

434 mm

Monochromatic Subaperture

Fig. 4.—Polychromatic beam footprint, including the full range of field angles, at the cross-disperser (*top*) and the elliptical monochromatic pupil from a single fiber (*bottom*).

using nonstandard wavelengths. This more careful calculation does not change our earlier conclusions based on ν_d, and we choose S-FSL5Y and PBM2Y for the zero-deviation prism pair. The properties of these two glasses are summarized in Table 1.

3.3. Prism Angles and Order Separation

The prism angles must be large enough to provide adequate cross-dispersion at the red end of the spectrum. We would like to maintain a minimum order separation of ~13 pixels (175 μm at the CCD), the interfiber separation in single-order multi-object operation. With Hectochelle's ~600 mm camera focal length, this corresponds to an angular deviation of ~1′. We can then establish the precise prism angles analytically or with a ray-tracing code. In Figure 5, we have plotted the interorder spacing as a function of wavelength for a variety of apex angles for the first prism ($\alpha = 40°$ in Fig. 1). The zero-deviation constraint sets the ratio of the first and second prism apex

TABLE 1
Properties of S-FSL5Y and PBM2Y Glasses

Property	S-FSL5Y	PBM2Y
Abbe number, ν_d[a]	70.3	36.3
Refractive index at 365.02 nm	1.50404	1.66635
Refractive index at 587.56 nm	1.48749	1.62004
Refractive index at 1013.98 nm	1.47915	1.60275
Coefficient of thermal expansion[b]	89×10^{-7}	86×10^{-7}

[a] $\nu_d \equiv (n_d - 1)/(n_F - n_C)$, where n_F, n_d, and n_C are the refractive indices at 486.1, 587.6, and 656.3 nm, respectively.
[b] Coefficient of thermal expansion valid between $-30°C$ and $70°C$.

angles. Here, we have used an undeviated wavelength of 550 nm, but the results depend only weakly on this value. If we extend Hectochelle's operation to 980 nm, a 40° apex angle is required to provide a 13 pixel interorder separation.

The interorder separation increases rapidly at the blue end of the spectrum, to a maximum of ~93 pixels (see Fig. 6). For observations requiring a limited spectral range, e.g., precision radial velocity studies in the 475–580 nm iodine cell absorption band, the interorder spacing will be relatively constant, so individual spectra can be interleaved to improve the filling factor. The red edge of the iodine band at 580 nm has an interorder spacing of ~39 pixels, so it will be possible to interleave the spectra of three individual objects.

Figure 7 shows the effect of unblocking every 17th fiber at the spectrograph entrance slit to properly separate groups of the six iodine band orders. Here we assume that an order-blocking filter that transmits only these six orders is used. The interorder spacing is more than required, and Figure 8 shows the effect of unblocking fibers in groups of three at the spectrograph entrance slit to use the extra space on the detector. For
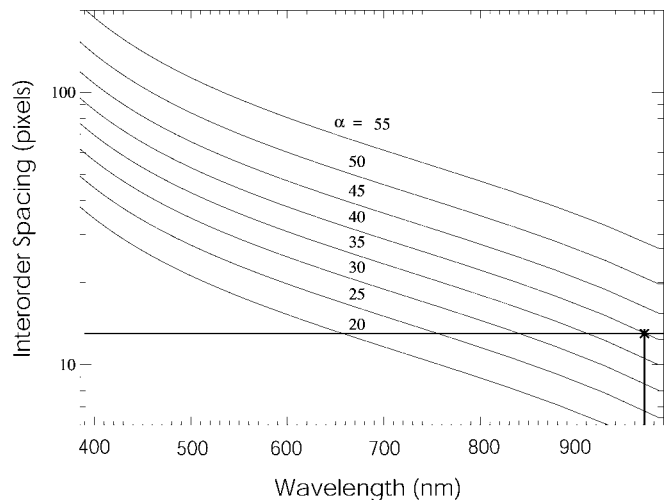
Interorder Spacing (pixels)

100

$\alpha = 55$
50
45
40
35
30
25
20

10

400   500   600   700   800   900

Wavelength (nm)

Fig. 5.—Interorder spacing as a function of wavelength for various apex angles of the first prism (α). The horizontal line indicates the minimum interorder spacing of 13 pixels, while the cross indicates the required $\alpha = 40°$ at 980 nm. This plot assumes a zero-deviation wavelength of 500 nm, but the results are only weakly dependent on this wavelength.
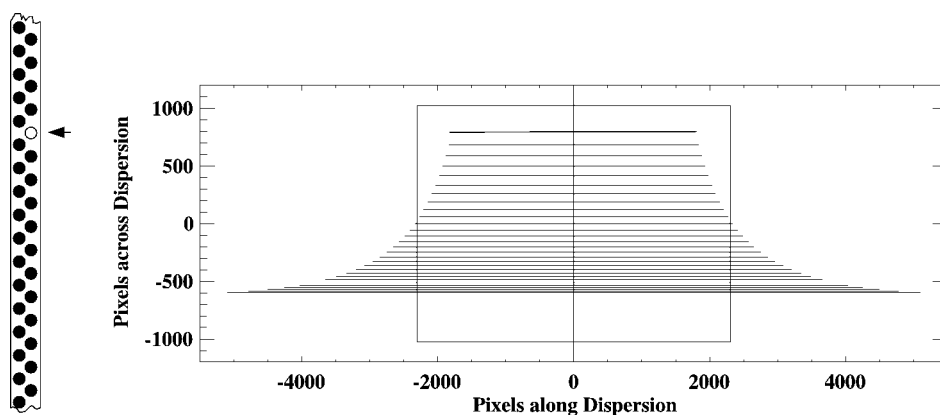
FIG. 6.—Echellogram for a single fiber at the full spectrograph passband (365–980 nm), not to scale. Orders redward of ~550 nm are longer than the CCD format. The fiber ends at the spectrograph entrance slit are schematically indicated on the left. The fiber ends plotted as filled circles are blocked. The format of one of Hectochelle's two CCDs, 2048 × 4608 pixels, is indicated by the superposed box in the top panel.

these precision radial velocity studies, interleaving will increase the multiplex advantage to ~42 from ~14.

3.4. Blue Transmission

The path lengths through the base of a large prism are long enough that internal absorption in the glass must be considered. Ignoring details of aperture or subaperture shape, the mean attenuation is given by

$$\overline{\alpha}(\lambda) = \frac{\int_0^{z_0} \alpha(l, \lambda)dz}{z_0} = \frac{\tau(\lambda)}{l_0}\left\{1 - e^{-l_0/\tau(\lambda)}\right\}, \qquad (2)$$

where $\alpha(l, \lambda)$ is the attenuation by the glass through path length l at a wavelength λ, l_0 is the path length across the base of the
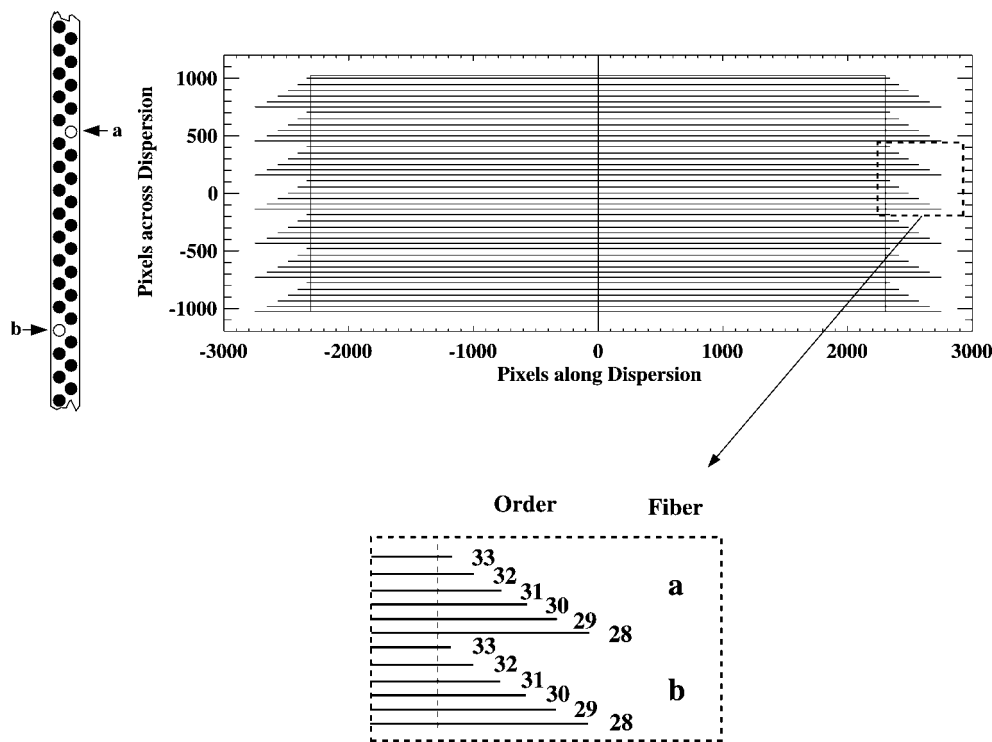

FIG. 7.—Echellogram in multiorder, multiobject mode for the iodine band orders (475–580 nm) on CCD format without interleaving. The fiber ends shown as filled circles on the left are blocked. Every 17th fiber is unblocked at the spectrograph entrance slit. The groups of six orders (selected with an appropriate filter) are properly spaced, but the interorder spacing is more than necessary. The format of one of Hectochelle's two CCDs, 2048 × 4608 pixels, is indicated by the superposed box in the top panel.
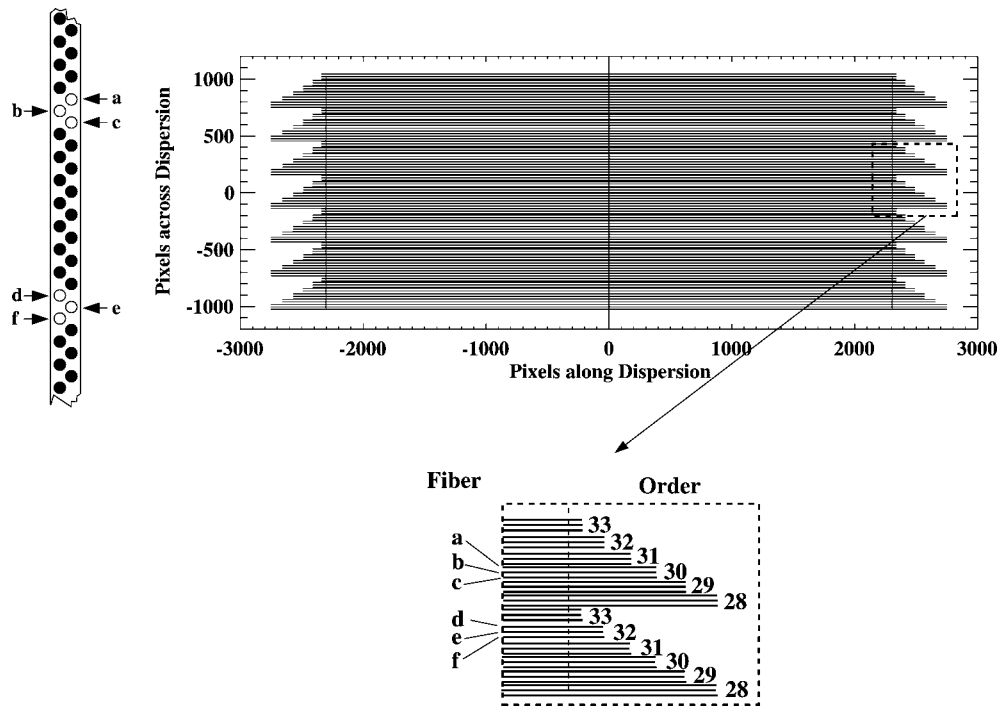
FIG. 8.—Echellogram in multiorder, multiobject mode for the iodine band orders (475–580 nm) on CCD format with interleaving. The fiber ends shown as filled circles on the left are blocked. Here, groups of three fibers are unblocked to use the extra space between orders for maximum multiplex advantage. The multiplex advantage is increased threefold. The format of one of Hectochelle's two CCDs, 2048 × 4608 pixels, is indicated by the superposed box in the top panel.

prism, z_0 is the height of the prism, and $\tau(\lambda)$ is the attenuation length of the glass at λ. Here we have made the simplification that the prism cross section is a right triangle; however, this does not affect the results for most useful prism geometries. The midplane approximation $\overline{\alpha}(\lambda) = e^{-\rho/2}$, where $\rho = l_0/\tau(\lambda)$, is accurate to better than 5%, even where $\rho = 1$.

Table 2 compares the transmissions of the two prism glasses at 365 nm, the blue limit of the Hectochelle, for a segmented and a monolithic prism cross-disperser design. A segmented design improves the transmission markedly for the PBM2Y prism half. The calculated total transmission of the Hectochelle cross-disperser is shown in Figure 9, where all known losses have been included.

4. SEGMENTED PRISM TOLERANCES AND MECHANICAL ISSUES

The pupil associated with each fiber image is spread over more than one segment of the cross-disperser. Errors in match-

TABLE 2
365 nm TRANSMISSION OF SEGMENTED AND MONOLITHIC PRISMS

	SEGMENTED		MONOLITHIC	
GLASS	Mean Path (mm)	Transmission	Mean Path (mm)	Transmission
PBM2Y	67	0.91	225	0.73
S-FSL5Y	85	0.99	271	0.97

ing the prism segment angles will therefore blur (or in extreme cases split) the monochromatic image of a fiber. As a result, perhaps the largest complication in using segmented prisms is the requirement to closely match their angular deviations. This requirement leads to relatively tight fabrication tolerances. These tolerances fall into three categories: (1) fabrication tolerances for the individual prisms that form the zero-deviation pairs, (2) bonding tolerances for assembling the zero-deviation pairs, and (3) alignment tolerances for the bonded prism segments. These errors are illustrated in Figures 10, 11, and 12.

With Hectochelle's camera focal length of ~600 mm, a beam deviation of 1″ corresponds to a displacement of 3 μm at the CCD. (A beam deviation of 1″ arises from a prism surface tilt of ~2″.) In order to maintain spectral resolution, the required tolerances in the dispersion direction of the echelle grating are tighter than those in the cross-dispersion direction. A monochromatic image of one of Hectochelle's 250 μm fibers at the CCD is a 112 μm × 64 μm ellipse, with the narrow dimension along the echelle's dispersion. In order to limit the degradation of the spectral resolution to 5%, the segment-to-segment induced blur (which we assume is added in quadrature to the intrinsic image diameter) must be kept below 20 μm, corresponding to a beam deviation of ~7″. If we adopt a looser 10% blur increase in the perpendicular direction, the segment-to-segment blur tolerance in that direction is 50 μm, corresponding to a beam deviation of ~17″.
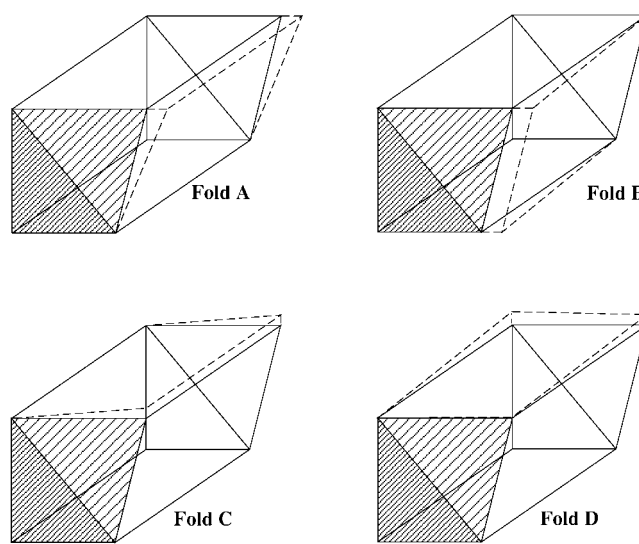
FIG. 10.—Potential fabrication errors of the individual prism elements that will cause segment-to-segment image blur.

direction, tilt B produces an error in the dispersion direction, and rot B produces a component in both directions. Adding together these fabrication and bonding errors, we find four terms that contribute in each direction. If each of these terms is allowed to contribute equally in quadrature, we require prism fabrication and bonding tolerances of ∼7″ for errors that cause blur in the dispersion direction, and ∼17″ for errors that cause blur in the cross-dispersion direction. If the errors are pessimistically assumed to add linearly, the tolerances tighten by a factor of 2.

Referring to equation (1) in § 3.2, we can calculate the errors that might arise from mixing glass from different melts. An
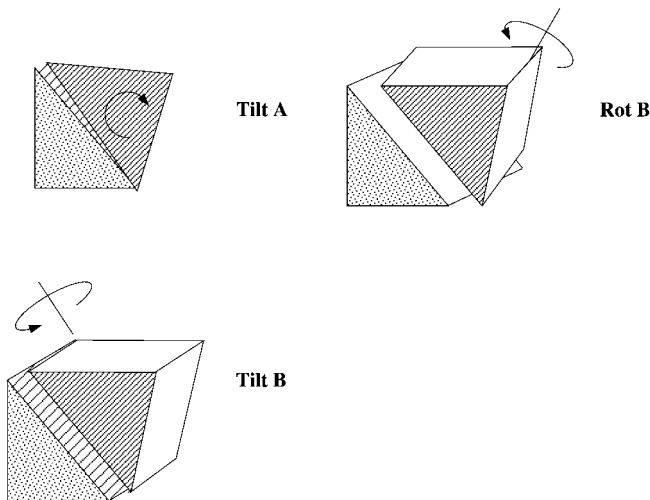

FIG. 11.—Potential bonding errors that result in misalignments between the prism pairs and segment-to-segment image blur.

FIG. 9.—*Top panel:* Transmission of Hectochelle's segmented cross-disperser, assuming Sol-gel antireflection coatings on both glass-air surfaces. *Bottom panel:* Throughput of the cross-dispersed Hectochelle. *Heavy solid line:* Peak throughput with cross dispersion but no order-separating filters. *Solid line:* Mean throughput with cross-dispersion but no order-separating filters. *Heavy dashed line:* Peak throughput with cross-dispersion and order-separating filters. *Dashed line:* Mean throughput with cross-dispersion and order-separating filters.

The relative alignments of the three bonded zero-deviation segments shown in Figure 12 are much less critical than the fabrication and bonding tolerances. Ray-tracing shows that tolerances of several arcminutes are acceptable. In any case, the bonded segments can be adjusted with shims, so these tolerances are not difficult to achieve.

Figure 10 illustrates four fabrication errors, but two of these, fold C and fold D, affect only segment-to-segment alignment and can be removed in the alignment procedure. Fold A affects image blur in the cross-dispersion direction, while fold B affects image blur in the dispersion direction. Each type of error is relevant for each prism component, so these fabrication errors contribute two deviation terms each. Figure 11 illustrates three bonding errors: tilt A produces an error in the cross-dispersion
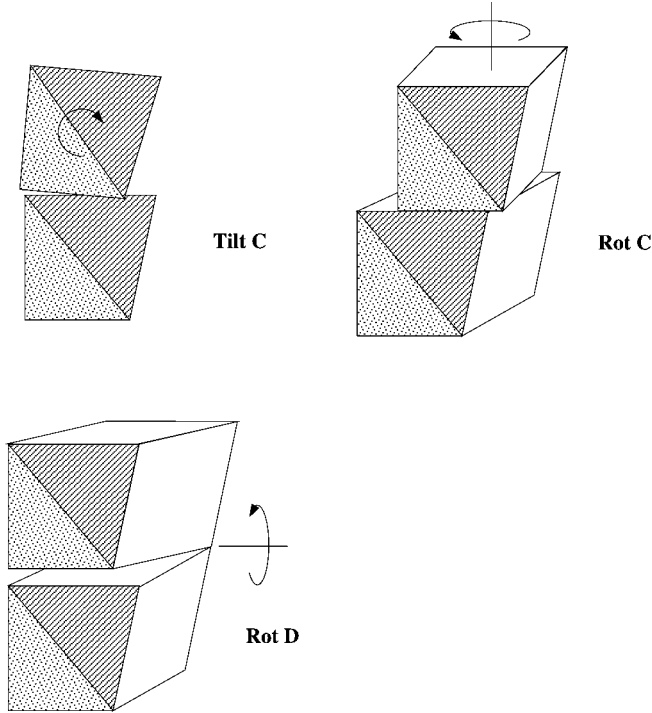
FIG. 12.—Potential alignment errors of the bonded prism segments. These can be reduced to negligible levels using straightforward alignment techniques.

upper limit to the melt-to-melt deviation is a refractive index change of 0.001. If we assume that the refractive index changes are uncorrelated, the fractional error in the deviation angle is less than 0.003, a negligible effect. If the melt-to-melt refractive index changes are correlated at different wavelengths, the fractional error in the deviation angle will be yet smaller.

Each of the Hectochelle zero-deviation prism segments will weigh ~50 kg, yielding a total prism weight of ~150 kg. The cross-disperser assembly must be moved on and off the spectrograph bench, so we estimate that a structure of at least 150 kg weight will be required to support the prisms and maintain their co-alignment.

Our calculations indicate that the closely matched thermal expansion coefficients will lead to relatively small internal stresses from material mismatch in the prisms as the temperature is changed: 0.7 MPa for a 30°C temperature swing.

5. CONCLUSIONS

We have presented a novel design for a segmented, zero-deviation cross-disperser that converts a single-order echelle spectrograph into a versatile instrument that allows trade-offs between spectral coverage and multiplex. This cross-disperser design can be used with no modifications to the existing spectrograph layout; the alignment of the spectrograph will not be disturbed by insertion of the cross-disperser. Our Hectochelle design uses three 50 kg segments, but thinner and lighter segments could be used at the expense of greater vignetting at the gaps between segments. This design might prove to be practical for other high-dispersion, fiber-fed spectrographs.

REFERENCES

Szentgyorgyi, A. H., Cheimets, P., Eng, R., Fabricant, D. G., Geary, J. C., Hartmann, L., Pieri, M. R., & Roll, J. B. 1998, Proc. SPIE, 3355, 242

Vogt, S. S. 1987, PASP, 99, 1214
Vogt, S. S., et al. 1994, Proc. SPIE, 2198, 362
Walker, D., Diego, F., & Bingham, R. G. 1990, Proc. SPIE, 1235, 535